Limits on runoff episode duration for early Mars: integrating lake hydrology and climate models

Gaia Stucky de Quay[1,2], Timothy A. Goudge[1,2], Edwin S. Kite[3], Caleb I. Fassett[4], and Scott D. Guzewich[5]

[1]Jackson School of Geosciences, University of Texas at Austin, Austin, Texas 78712, USA
[2]Center for Planetary Systems Habitability, University of Texas at Austin, Austin, Texas 78712, USA
[3]Department of the Geophysical Sciences, University of Chicago, Chicago, Illinois 60637, USA
[4]NASA Marshall Space Flight Center, Huntsville, Alabama 35805, USA
[5]NASA Goddard Space Flight Center, Greenbelt, Maryland 20771, USA

Key Points:

- Coupled lake system morphologies were combined with climate model outputs to quantify upper and lower limits on runoff episode durations.
- Breaching runoff episodes lasted 10^2-10^5 yr depending on models and are spatially variable; other episodes could be shorter but not longer.
- Our constraints on lake persistence may be tested through *in situ* observations made by the Mars 2020 Perseverance rover in Jezero crater.

Corresponding author: Gaia Stucky de Quay, g.stucky@utexas.edu

Abstract

Fluvio-lacustrine features on the martian surface attest to a climate that was radically different in the past. Since climate models have difficulty sustaining a liquid hydrosphere at the surface, multiple cycles of runoff episodes may have characterized the ancient Mars climate. A fundamental question thus remains: what was the duration of these runoff-producing episodes? Here we use morphometric measurements from newly identified coupled lake systems (containing both an open- and a closed-basin lake). We combined hydrological balances with precipitation outputs from climate models, and found that breaching runoff episodes likely lasted $10^2 - 10^5$ yr; other episodes may have been shorter but could not be longer. Runoff episode durations are model-dependent and spatially variable, and no climate model scenario can satisfy a unique duration for all coupled systems. In the near future, these quantitative constraints on early Mars lake persistence may be tested through *in situ* observations from Perseverance rover.

1 Introduction

Constraining the duration of periods for which liquid water was present on the surface of Mars has remained a fundamental challenge since evidence for ancient fluvial activity was first discovered (Carr, 1987; Wordsworth, 2016; Kite, 2019). In addition to informing our understanding of planetary and climatic evolution, these hydrologic timescales have profound implications for potential habitability beyond Earth. Yet, the persisting difficulty in quantifying past timescales is two-fold. First, the duration of Mars' early hydroclimate can be assessed via different approaches, namely geomorphic analyses (e.g., Hoke et al., 2011), numerical climate models (e.g., Ramirez et al., 2020), or chemical alteration studies (e.g., Bishop et al., 2018). Although this should ideally work as an advantage, general agreement between these approaches is often lacking. Second, it is unlikely that a single, uniform ancient climate existed. Instead, early Mars was probably characterized by a dynamic climate with runoff episodes varying at shorter length- and timescales, as suggested by layered deposits, valley morphologies, semi-arid basin hydrology, and weak aqueous alteration, among others (e.g., Malin & Edgett, 2000; Barnhart et al., 2009; Matsubara et al., 2011; Ehlmann et al., 2011, respectively). Hence, convergence towards a constrained timescale solution requires not only an improved understanding of the spatio-temporal complexity of the hydroclimate, but also a shift towards viewing different timescale-deducing methods as complementary rather than contrasting.

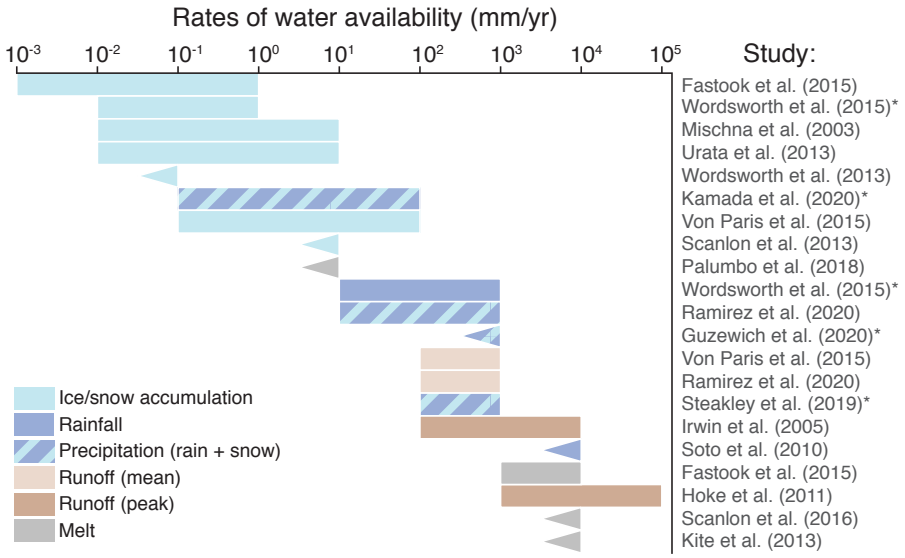

Figure 1. Range of water availability rates for early Mars from previous studies. Runoff rates are derived from geological observations and all other rates are from (climate/glacial) numerical models. Model outputs indicated with an asterisk are used in this work. Values are rounded to the nearest order of magnitude (see Supplementary Tables S1 and S2).

In general, most geomorphic evidence suggests a wet climate lasting at least 10 kyr, and perhaps 100 Myr, up to the Noachian-Hesperian boundary ($\gtrsim$ 3.7 Ga), whether inferred from erosional (e.g., Craddock & Howard, 2002; Barnhart et al., 2009) or depositional (e.g., Armitage et al., 2011; Schon et al., 2012; Grotzinger et al., 2015) systems. In order to align these geomorphic constraints with hydroclimatic limits set by geochemical records and climate models, it is often proposed that surface liquid water was episodic, although the mechanism behind this episodicity remains uncertain (Wordsworth, 2016; Kite, 2019). An important point that goes into this hypothesis is that geomorphic timescales are cumulative, i.e., they record the total amount of time taken to create a landform, whether a bedrock valley or fan deposit. As such, these studies typically rely on assumptions for runoff intermittency to calculate total durations (e.g., Buhler et al., 2014). If no hiatuses are considered, local depositional timescales could be substantially shorter (1-100 yr; e.g., Jerolmack et al., 2004; Fassett & Head, 2005; Kleinhans et al., 2010). Further, calculated water availability rates, such as precipitation, runoff, and melting rates, vary over several orders of magnitude (Figure 1); these estimates are not only sensitive to the methodology used, but also the spatial and temporal resolution employed. Clearly, there remains a need

to shed further light on the uninterrupted availability of liquid water on the martian surface. Here we aim to provide new insights into this problem by addressing the following question: how can we constrain the duration of a single runoff episode?

Our approach focuses on valley network-fed paleolakes, which provides a unique opportunity to assess individual surface runoff episodes: a discrete episode of time with net average positive runoff (i.e., runoff rate exceeds any losses; Supplementary Figure S1). Lake systems fall into one of two broad hydrological categories: open- or closed-basins (Cabrol & Grin, 1999, 2001; Fassett & Head, 2008; Goudge et al., 2015, 2016). Open-basin lakes accumulated enough water to overflow and erode an outlet canyon (e.g., Goudge et al., 2019), whereas closed-basin lakes did not. As such, the presence or absence of an outlet canyon directly records whether a threshold event—lake overspill—was achieved in any single runoff episode (Figure S1; Supplementary Text S1). Water input cannot be considered cumulative if separated by periods of water loss. In this work we capitalize on this threshold relationship by investigating newly identified coupled lake systems, which contain both an open- and a closed-basin lake that are hydrologically connected (Figure 2a; Stucky de Quay et al., 2020). By combining these new geological constraints with a suite of runoff rates from existing climate models, we are able to place new limits on runoff episode duration across the surface of ancient Mars.

2 Methodology

2.1 Paleolake geometry mapping

We investigated a subset of valley network-fed coupled paleolakes from Stucky de Quay et al. (2020), which, for both open- and closed-basin lakes contained within a coupled system, provide lake basin area (A_L), lake basin volume (V_L), and watershed area (A_W; Figure 2b). We used 7 coupled lake systems from this morphologic database (Supplementary Figure S2; Table S3) and measured an additional fourth parameter for all systems: lake volume remaining after the open-basin lake breached and drained, V_R. This was done by identifying the highest closed contour in the basin before it spilled into the outlet canyon (e.g., Fassett & Head, 2008). For this we used the ∼100 m/pixel global daytime infrared mosaic (Edwards et al., 2011) from the Thermal Emission Imaging System (THEMIS; Christensen et al., 2004), and ∼463 m/pixel Mars Orbiter Laser Altimeter global gridded elevation data (MOLA; Smith et al., 2001). Subsequently, coupled systems were classified as either embedded (where

the open-basin lake is contained within the watershed of the closed-basin lake watershed; n=6) or adjacent (where the open- and closed-basin lake watersheds share drainage divides; n=1). Importantly, sediment deposition—before, during, or after lake filling—is unlikely to significantly affect measured basin morphologies (see Supplementary Text S2; Mangold et al., 2009).

2.2 Derivation of lake hydrological balance

Paleolake hydrology can be expressed using standard water balance equations (Horton, 1943; Benson & Thompson, 1987; Howard, 2007; Fassett & Head, 2008; Matsubara et al., 2011). In a simplified system, the total lake volume, V_L, accumulated over a runoff episode of duration, T, is given by

$$V_L = ((A_L + A_W)P - (A_L)E)T, \tag{1}$$

where P is average rainfall and/or snowmelt rates and E is average evaporation rate. Since lakes are fed by valley networks (Figure 1; Figure S2), this implies they were predominantly fed by surface runoff, and groundwater infiltration is likely to have limited effect on hydrology (see Stucky de Quay et al., 2020). In an embedded coupled system where an upstream open-basin lake (O) breaches at a time, T_B, and overflows into a downstream closed-basin lake (C), and assuming a steady and uniform precipitation rate, we can express both lake volumes as a function of time, t:

$$v_O = \begin{cases} V_{L,O}\left(\dfrac{t}{T_B}\right) & \text{if } t \leq T_B; \\ V_R & \text{if } t > T_B; \end{cases} \tag{2}$$

$$v_C = \begin{cases} (A_{W,C} - XA_{L,C})\dfrac{V_{L,O}}{A_{W,O} - XA_{L,O}}\left(\dfrac{t}{T_B}\right) & \text{if } t \leq T_B; \\ (A_{W,O} + A_{W,C} - XA_{L,O} - XA_{L,C})\dfrac{V_{L,O}}{A_{W,O} - XA_{L,O}}\left(\dfrac{t}{T_B}\right) - V_R & \text{if } t > T_B, \end{cases} \tag{3}$$

where the full derivation is provided in Supplementary Text S3. Here, X denotes the aridity of the system, and can be expressed as $(\frac{1}{\mathrm{AI}} - 1)$, where the aridity index, AI, is the ratio of runoff to evaporation (P/E; Matsubara et al., 2011; Stucky de Quay et al., 2020). Because closed-basin lakes did not overflow, the observed basin volume provides an upper limit for v_C, i.e., v_C in equation (3) cannot exceed $V_{L,C}$. These expressions allow us to assess the permitted timescales for runoff generation, which must be greater than the breaching timescale, T_B, but less than the maximum timescale, T_{max} (where $v_C[T_{max}] = V_{L,C}$; see Figure S1).

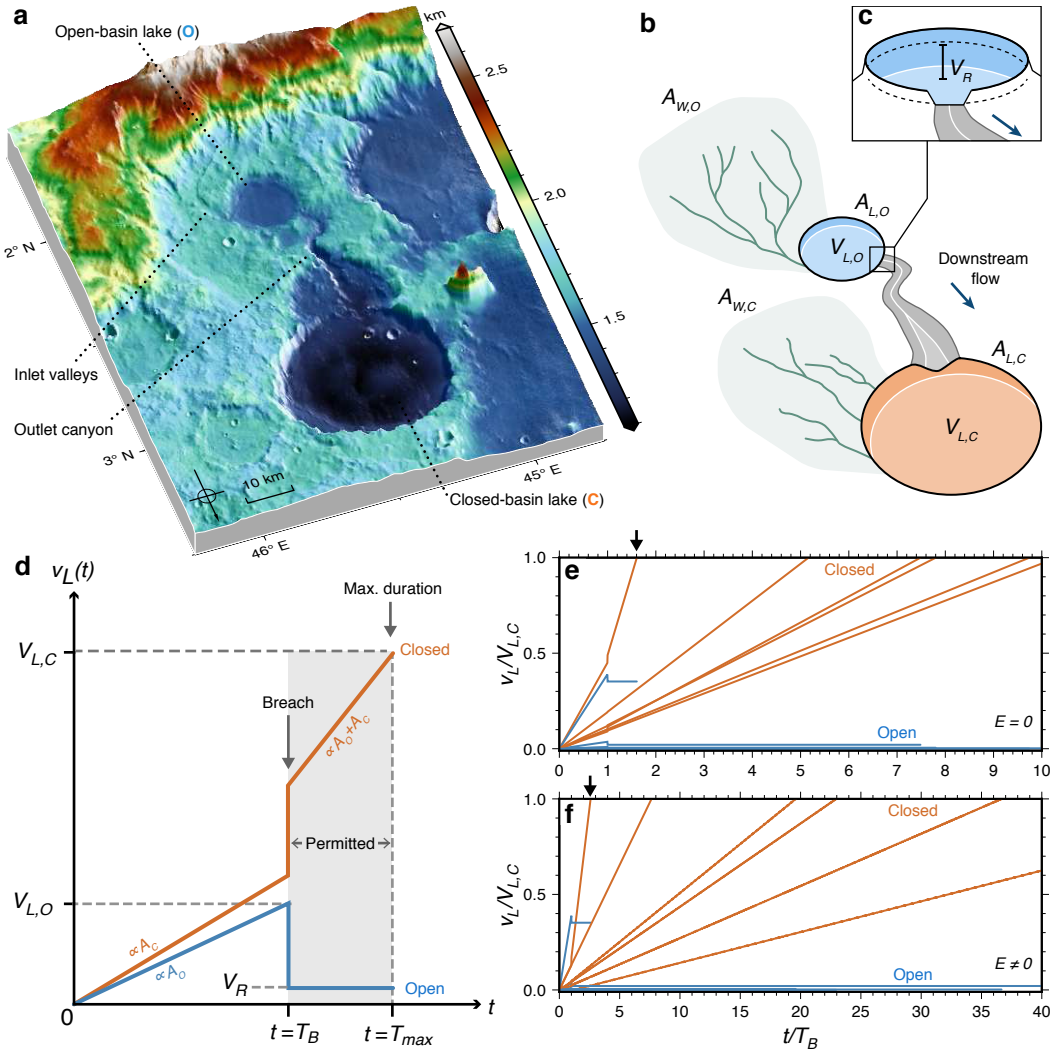

Figure 2. (a) Example of a coupled lake system on Mars (Basin ID 185/89; Table S3). Images and elevation data are from THEMIS and MOLA, respectively. (b) Schematic diagram of key lake morphometric measurements. Blue polygon = open-basin lake (O) with area $A_{L,O}$ and volume $V_{L,O}$; orange polygon = closed-basin lake (C) area $A_{L,C}$ and volume $V_{L,C}$. Green shaded area = watershed areas, $A_{W,O}$ and $A_{W,C}$) where dark green=inlet valleys. Grey polygon = outlet canyon. (c) Schematic of remaining lake volume V_R after breach and outlet erosion (Figure 2c). (d) Simple model for lake volume changes over time following equations (2) and (3). Gray shaded region denotes the permitted runoff episode duration between breaching (T_B) and the maximum duration set by the volume of the closed-basin lake (T_{max}). Here, $A_O = A_{W,O} + A_{L,O}$ and $A_C = A_{W,C} + A_{L,C}$ for simplicity. (e) and (f) show results using our 6 embedded coupled systems, where (e) considers no evaporation, and (f) applies an aridity index, AI, of ~ 0.26. Here, time (x-axis) is normalized to the breach event, T_B, and volume (y-axis) is normalized to the volume of each individual closed-basin lake ($V_{L,C}$). Black arrow = the shortest T_{max}/T_B value, indicating the most restrictive case.

Figure 2d shows the predicted changes in lake volume for open- and closed-basin lakes schematically following equations (2) and (3). Both lakes fill at a rate proportional to their initial catchment size. At $t = T_B$, a breach occurs in the upstream open-basin lake and the drained volume is transferred downstream into the closed-basin lake. After the breach, the open-basin lake volume remains constant and the closed-basin lake has a higher filling rate equivalent to the combined catchments of both lakes (since inflow and outflow in the upstream open-basin lake are now balanced). Without independent constraints, these runoff episode limits can only be constrained relative to the breaching timescale.

2.3 Temporal constraints using climate models

To provide absolute constraints on the runoff episode duration, we derived the lower, T_B, and upper, T_{max}, limits by building on the expressions provided above (equations 1-3; Text S3; Figure S1). For a given embedded coupled system containing an open- and closed-basin lake, the runoff episode limits are given as

$$T_B = \frac{V_{L,O}}{(A_{W,O} - XA_{L,O})P}; \tag{4}$$

$$T_{max} = \frac{V_{L,C} + V_R}{(A_{W,O} + A_{W,C} - XA_{L,O} - XA_{L,C})P}. \tag{5}$$

To explicitly solve for these durations, we use precipitation rates from existing climate model outputs as a proxy for P. Out of the existing constraints outlined in Figure 1, we selected precipitation rate outputs from four global climate models based on data availability and their full coverage of the planet (Figures 3a-d; Wordsworth et al., 2015; Steakley et al., 2019; Kamada et al., 2020; Guzewich et al., 2021). For each coupled lake system, we extracted the average value for P within the total lake watershed using outputs from each of the models (Figure 3e). Note that each model considered various different scenarios, resulting in a total of 16 model outputs (Supplementary Table S4). This provides, for each coupled lake system, a range of durations that are permitted both by its morphology and the regional, model-dependent runoff rate.

3 Results

3.1 Relative runoff episode limits

The geometries of paleolakes allow us to assess a range of timescales for which a given coupled system could have remained active after breaching of the open-basin lake. Figures

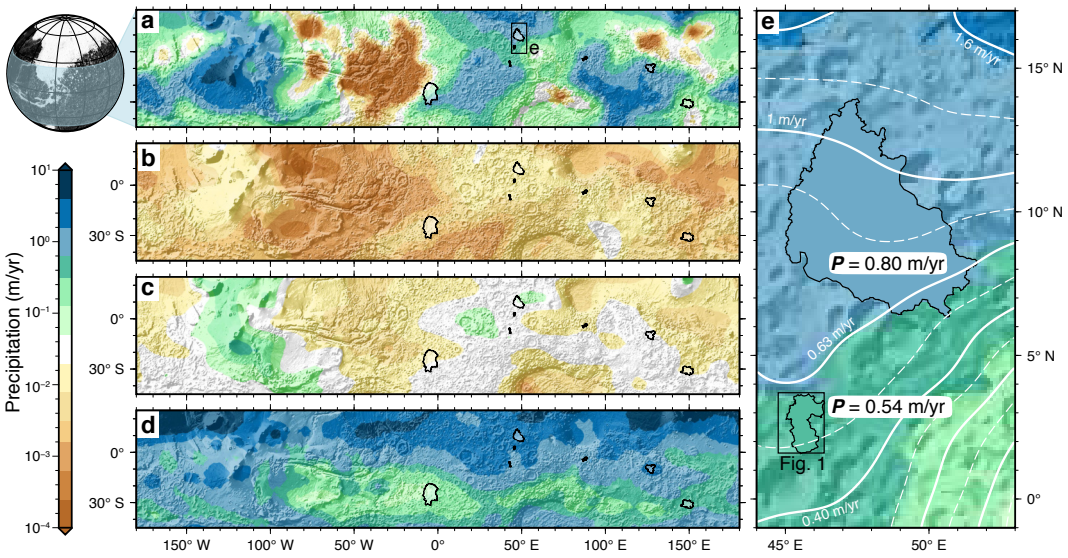

Figure 3. Precipitation rates from global climate models and watershed data extraction. Four climate model outputs are shown: (a) Warm and wet climate from Wordsworth et al. (2015). Note location of panel (e). (b) 0.5 bar atmosphere scenario from Kamada et al. (2020). (c) 10 m global equivalent layer (GEL) of water at 25° obliquity from Guzewich et al. (2021). (d) An impact-heated atmosphere generated by a 50 km-diameter impactor from Steakley et al. (2019). Table S4 lists all 16 climate scenarios. Black polygons = total watershed of lake systems. Latitudes and longitudes are the same for (a)-(d). (e) Example calculation of regional runoff rate, P, for each system, which is averaged across the combined watershed and lake area. Hillshade from MOLA topography.

2e,f show the relative runoff episode durations that are permitted for all 6 embedded coupled systems. Note that only values between $t = T_B$ and T_{max} (i.e., gray shaded region in Figure 2d) are permitted; hence, systems with a large value of T_{max}/T_B have a wide range of permitted runoff episode durations, whereas systems that have $T_{max}/T_B \rightarrow 1.0$ imply a narrow range of permitted timescales relative to breaching. Values for T_{max}/T_B range from 1.6 to 10 if we assume no evaporation occurs (Figure 2e). If we assume a more realistic semiarid regime, with AI ~ 0.26 (from Stucky de Quay et al., 2020), then T_{max}/T_B ranges between 2.6 to 63 (Figure 2f).

These results suggest that, for the most tightly constrained system (i.e., the lowest T_{max}/T_B value; black arrow in Figure 2e,f), runoff generation can only continue for $\sim 1.6-2.6$ longer than the time it took to initially breach the open-basin lake. For this system (Basin ID 187/9; Table S3), the open-basin lake spends a minimum of $\sim 40\%$ of the runoff

episode duration filling up before it breaches. Systems with larger T_{max}/T_B values may not require runoff cessation shortly after breaching, but do not explicitly preclude it. As a result, open lake systems on Mars may spend a large portion of their evolution filling up as closed lakes, as opposed to as stable open lakes.

3.2 Distribution of absolute runoff episode durations

Using equations (4) and (5), we solved for T_B and T_{max} for each of the seven coupled systems using existing P values extracted from global climate models (Figure 3; Table S4). The resultant distributions for the runoff episode durations are shown in Figure 4. Each panel in Figure 4 illustrates the number of coupled systems with T_B and T_{max} values that bound the episode duration, T, specified on the x-axis (i.e., systems where $T_B \leq T < T_{max}$ is satisfied) for that climate scenario. As a reference, Figure 4a shows the permitted temporal distributions if we assume globally constant runoff rates from geological observations by Irwin et al. (2005). Here, a 10,000 yr runoff episode duration only satisfies one coupled system if the runoff rate was 60 mm/d, but would satisfy three systems if it was 1 mm/d. Each remaining panel (b-f) shows the timescale distributions for four different global climate studies, including different scenarios within each to explore how various parameters affect timescale distributions (Table S4). Notably, none of the models satisfy all 7 coupled systems for a single duration bin (see Section 4.1).

Figure 4b compares timescales using two end-member precipitation scenarios for rainfall and snowfall (wet, warm at 1.0 bar vs. cold, icy at 0.6 bar, respectively, from Wordsworth et al., 2015). Figure 4c shows the effect of increasing surface pressure (from 0.5 to 2.0 bar; Kamada et al., 2020). Climate scenarios with higher pressures, and consequently greater rainfall, generally result in shorter timescales, except for the highest surface pressure of 2.0 bar, where timescales increase. Using model outputs from Guzewich et al. (2021), we find that higher obliquities result in reduced runoff episode durations; however, global equivalent water inventory size has negligible effects (Figures 4d,e). Finally, durations required for an impact-induced atmosphere in Figure 4f show that impactor size does not significantly affect the distributions (50 and 100 km-diameter; Steakley et al., 2019). The distributions in Figure 4 assume a semiarid regime with AI $\sim$ 0.26, however results with no evaporation are also shown in Supplementary Figure S3, suggesting less than an order of magnitude difference.

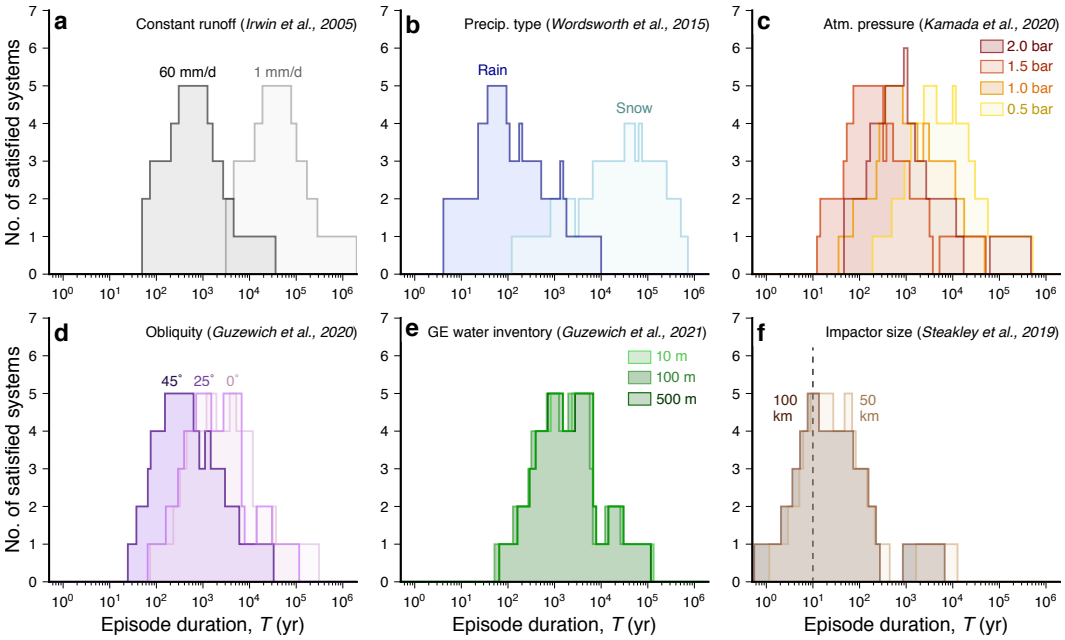

Figure 4. Distribution of runoff episode durations that satisfy the 7 studied coupled systems using different runoff constraints: (a) Spatially constant runoff rate (Irwin et al., 2005); (b)–(f) Precipitation rate outputs from different climate models/scenarios as indicated above each panel (Table S4); GE = global equivalent; precip. = precipitation; atm. = atmospheric; dashed line in (f) = limit of 10 years, the duration for which cumulative precipitation was estimated in the impact heating scenario.

4 Discussion & Conclusion

4.1 Implications for ancient hydroclimate scenarios

The mere existence of coupled lake systems implies that runoff generation was sufficiently intense and/or prolonged such that the contained open-basin lake breaches, but not enough to breach the downstream closed-basin lake (Figure 2). Unlike most terrestrial systems, these lakes would be less capable of achieving steady-state because the flat-floored, steep-walled crater basins would not allow lake area to continually increase until enhanced evaporation could offset runoff input. These systems thus point to a climate regime that comprises lake filling and overflow, followed—sometimes shortly—by runoff cessation, all within the timeframes indicated by Figure 4.

Overall, the shortest runoff episode durations (<1 yr) are observed for the 100 km-diameter impact heating scenario from Steakley et al. (2019), whereas the longest durations

correspond to Wordsworth et al. (2015)'s snowfall scenario (up to 10^6 yr; see following section for discussion on snowfall vs. snowmelt). In addition to the relative position of each distribution in Figure 4, both the width and height of each individual distribution provide further information. The wider the distribution, the larger the total range of timescales that are permitted by coupled lake hydrology. The taller the distribution (where maximum = 7), the greater the number of lakes that are satisfied by any given runoff episode duration bin. As such, the peak of each distribution denotes the T bin that satisfies the most coupled lake systems. If all systems were formed in runoff episodes of similar durations, then this peak T bin corresponds to the most probable duration for that climate scenario's distribution.

Distributions of T tend to span 3–4 orders of magnitude, suggesting a wide range of permissible timescales for all scenarios. When assessing the distribution peaks, we find that no single T bin can satisfy all 7 coupled systems for any scenario. Most scenarios can satisfy up to 5 systems, with the two exceptions being the 2.0 bar scenario from Kamada et al. (2020), which satisfies 6 systems for $T \sim 1000$ yr, and the Wordsworth et al. (2015) snowfall scenario which only satisfies 4 at most (Figure 4). In general, most distribution peaks lie between 100 – 10,000 yr, suggesting this range of breaching episode duration satisfies the greatest number of coupled system hydrologic constraints across the planet. Importantly, other runoff episodes (either before or after the breaching episode; Figure S1) could have been shorter, but no episode could exceed the maximum durations at any point in during early Mars' history, since closed-basin lakes did not overflow.

4.2 Runoff rates and the geological record

Global climate models provide valuable quantitative inputs for assessing runoff rates required to fill our lake systems as a function of space. Although geological estimates are important for understanding reach-scale, channel-forming hydrology, they are more challenging to extend over regional- to global-scales precisely due to being both localized and related to peak hydrologic conditions (Figure 1; Table S2). For example, at first glance runoff rates modeled by Steakley et al. (2019) most closely match those estimated from geomorphic observations (Figure 1). However, such an impact-heated atmosphere can only persist for a maximum ∼10 yr (Steakley et al., 2019; Turbet et al., 2020), and systems requiring longer time periods are not permissible. Despite this cut-off, the runoff rates provided are sufficient to fill the lakes, and are able to satisfy 5 systems for a runoff episode duration ∼10 yr (Figure 4f). Importantly, though, for discrete events such as an impact,

it seems most likely that T was spatially homogeneous, as it would reflect a global heating event.

Aside from the precipitation models used in this study (Figure 4), others have also explored snowfall or ice accumulation rates as a function of space (Figure 1). These snow/ice accumulation distributions are commonly compared to locations of fluvio-lacustrine features such as valley networks (e.g., Wordsworth et al., 2015). However, the relationship between snow accumulation and subsequent runoff rates is not well understood, and variability in processes such as snow ablation could result in spatial discrepancies between snowfall and resulting runoff. Other studies have derived snowmelt production rates (Figure 1), however, when calculated in global models they have yet to generate sufficient runoff in the required mid-latitude regions (e.g., Palumbo & Head, 2018). This could explain why the snowfall distribution in Figure 4b satisfies less systems than all other models for a single time bin, since the duration of liquid water availability (e.g., snowmelt) may not be directly related to snow/ice accumulation at any given location.

4.3 Lake persistence and episodic climate forcing

Despite the wide range of climate scenarios invoked, our runoff episode durations are broadly in agreement with previous estimates for lake filling and ponding of $\sim 10^2 - 10^4$ yr (Melas Chasma and Gale Crater; Williams & Weitz, 2014; Palucis et al., 2016, respectively). However, these younger lakes postdate the Noachian-Hesperian boundary and thus may not reflect similar climate conditions. The sparsity of well-preserved fluvial deposits in older, valley network-fed lake basins results in limited independent geological constraints on lake persistence to test our results. Nonetheless, estimates for total delta building timescales have been previously calculated for two valley network-fed basins: Eberswalde (a potential closed-basin lake) and Jezero (an open-basin lake). For Eberswalde, total delta-building runoff duration could have lasted $10^4 - 10^6$ yr (Moore et al., 2003; Irwin et al., 2015), with maybe a lake persisting for $> 10^5$ yr (Bhattacharya et al., 2005). Other studies have suggested total delta-building runoff durations as short as $10^1 - 10^2$ yr (Jerolmack et al., 2004; Lewis & Aharonson, 2006). For Jezero crater, total delta-building duration estimates have similarly ranged from $10^1 - 10^3$ yr (Fassett & Head, 2005; Salese et al., 2020; Lapôtre & Ielpi, 2020). However, because we do not know what fraction of a runoff episode is spent building a sedimentary deposit, these constraints are difficult to compare. Future insights into lake level persistence and variability, as captured by delta aggradation

and progradation, can hopefully be obtained as the Mars 2020 Perseverance rover explores Jezero crater, providing key independent constraints to test our results.

How do our episode duration estimates fit into the bigger picture of Mars' paleoclimate? Previous studies of valley network evolution suggest that early Mars was characterized by a long-lived runoff-producing climate lasting $> 10^5$ yr, assuming some intermittency frequency (Barnhart et al., 2009; Hoke et al., 2011). Our estimated durations suggest runoff production occurred in individual episodes lasting $10^2 - 10^5$ yr, separated by periods of water loss sufficiently long to reset the lake systems. As such, a large number of these individual runoff episodes likely comprised the total runoff-producing climate, interspersed by periods of negligible runoff. This is broadly consisent with mineralogical records suggesting wet climates were punctuated by long hyperarid intervals (Ehlmann & Edwards, 2014), as well as the presence of deeply incised inlet valleys that fed our paleolake database (Figure S2), implying multiple cycles of runoff and erosion (e.g., Rosenberg & Head, 2015; Luo et al., 2017). Ultimately, our lake-filling runoff episodes likely occurred during favorable climatic conditions associated with extremes of perhaps quasi-cyclical climate changes on Mars. Whether this cyclicity was modulated through astronomical variability (e.g., obliquity; Toon et al., 1980), geologically-derived fluctuations (e.g., redox oscillations; Wordsworth et al., 2021), or other driving forces, an intermittent climate forcing that can generate multiple runoff episodes lasting hundreds to thousands of years would be needed in order to reconcile with the Late Noachian / Early Hesperian hydrological record on Mars.

Acknowledgments

This work was supported by NASA MDAP grant 80NSSC17K0442. This is UT CPSH contribution #XXXXX. We are grateful to Alejandro Soto, Arihiro Kamada, Kathryn Steakley, Michael Mischna, and Robin Wordsworth for helpful discussions and access to climate model outputs. Datasets are available from Wordsworth et al. (2015), Steakley et al. (2019), Kamada et al. (2020), and Guzewich et al. (2021).

References

Armitage, J. J., Warner, N. H., Goddard, K., & Gupta, S. (2011). Timescales of alluvial fan development by precipitation on Mars. *Geophysical Research Letters*, *38*(17).

Barnhart, C. J., Howard, A. D., & Moore, J. M. (2009). Long-term precipitation and late-stage valley network formation: Landform simulations of Parana Basin, Mars. *Journal of Geophysical Research: Planets*, *114*(E1).

Benson, L. V., & Thompson, R. S. (1987). Lake-level variation in the Lahontan Basin for the past 50,000 years. *Quaternary Research*, *28*(1), 69–85.

Bhattacharya, J. P., Payenberg, T. H., Lang, S. C., & Bourke, M. (2005). Dynamic river channels suggest a long-lived Noachian crater lake on Mars. *Geophysical Research Letters*, *32*(10).

Bishop, J. L., Fairén, A. G., Michalski, J. R., Gago-Duport, L., Baker, L. L., Velbel, M. A., ... Rampe, E. B. (2018). Surface clay formation during short-term warmer and wetter conditions on a largely cold ancient Mars. *Nature Astronomy*, *2*(3), 206–213.

Buhler, P. B., Fassett, C. I., Head, J. W., & Lamb, M. P. (2014). Timescales of fluvial activity and intermittency in Milna Crater, Mars. *Icarus*, *241*, 130–147.

Cabrol, N. A., & Grin, E. A. (1999). Distribution, classification, and ages of Martian impact crater lakes. *Icarus*, *142*(1), 160–172.

Cabrol, N. A., & Grin, E. A. (2001). The evolution of lacustrine environments on Mars: Is Mars only hydrologically dormant? *Icarus*, *149*(2), 291–328.

Carr, M. H. (1987). Water on mars. *Nature*, *326*(6108), 30–35.

Christensen, P. R., Jakosky, B. M., Kieffer, H. H., Malin, M. C., McSween, H. Y., Nealson, K., ... others (2004). The thermal emission imaging system (THEMIS) for the Mars 2001 Odyssey Mission. *Space Science Reviews*, *110*(1-2), 85–130.

Craddock, R. A., & Howard, A. D. (2002). The case for rainfall on a warm, wet early Mars. *Journal of Geophysical Research: Planets*, *107*(E11), 21–1.

Edwards, C., Nowicki, K., Christensen, P., Hill, J., Gorelick, N., & Murray, K. (2011). Mosaicking of global planetary image datasets: 1. Techniques and data processing for Thermal Emission Imaging System (THEMIS) multi-spectral data. *Journal of Geophysical Research: Planets*, *116*(E10).

Ehlmann, B. L., & Edwards, C. S. (2014). Mineralogy of the Martian surface. *Annual Review of Earth and Planetary Sciences*, *42*.

Ehlmann, B. L., Mustard, J. F., Murchie, S. L., Bibring, J.-P., Meunier, A., Fraeman, A. A., & Langevin, Y. (2011). Subsurface water and clay mineral formation during the early history of Mars. *Nature*, *479*(7371), 53–60.

Fassett, C. I., & Head, J. W. (2005). Fluvial sedimentary deposits on Mars: Ancient deltas in a crater lake in the Nili Fossae region. *Geophysical Research Letters*, *32*(14).

Fassett, C. I., & Head, J. W. (2008). Valley network-fed, open-basin lakes on Mars: Distribution and implications for Noachian surface and subsurface hydrology. *Icarus*, *198*(1), 37–56.

Fastook, J. L., & Head, J. W. (2015). Glaciation in the Late Noachian Icy Highlands: Ice accumulation, distribution, flow rates, basal melting, and top-down melting rates and patterns. *Planetary and Space Science*, *106*, 82–98.

Goudge, T. A., Aureli, K. L., Head, J. W., Fassett, C. I., & Mustard, J. F. (2015). Classification and analysis of candidate impact crater-hosted closed-basin lakes on Mars. *Icarus*, *260*, 346–367.

Goudge, T. A., Fassett, C. I., Head, J. W., Mustard, J. F., & Aureli, K. L. (2016). Insights into surface runoff on early Mars from paleolake basin morphology and stratigraphy. *Geology*, *44*(6), 419–422.

Goudge, T. A., Fassett, C. I., & Mohrig, D. (2019). Incision of paleolake outlet canyons on Mars from overflow flooding. *Geology*, *47*(1), 7–10.

Grotzinger, J., Gupta, S., Malin, M., Rubin, D., Schieber, J., Siebach, K., ... others (2015). Deposition, exhumation, and paleoclimate of an ancient lake deposit, Gale crater, Mars. *Science*, *350*(6257).

Guzewich, S. D., Way, M., Aleinov, I., Wolf, E. T., Del Genio, A. D., Wordsworth, R. D., & Tsigaridis, K. (2021). 3D Simulations of the Early Martian Hydrological Cycle Mediated by a H2-CO2 Greenhouse. *Earth and Space Science Open Archive*, 47.

Hoke, M. R., Hynek, B. M., & Tucker, G. E. (2011). Formation timescales of large Martian valley networks. *Earth and Planetary Science Letters*, *312*(1-2), 1–12.

Horton, R. E. (1943). Hydrologic interrelations between lands and oceans. *Eos, Transactions American Geophysical Union*, *24*(2), 753–764.

Howard, A. D. (2007). Simulating the development of Martian highland landscapes through the interaction of impact cratering, fluvial erosion, and variable hydrologic forcing. *Geomorphology*, *91*, 332–363.

Irwin, R. P., Craddock, R. A., & Howard, A. D. (2005). Interior channels in Martian valley networks: Discharge and runoff production. *Geology*, *33*(6), 489–492.

Irwin, R. P., Lewis, K. W., Howard, A. D., & Grant, J. A. (2015). Paleohydrology of Eberswalde crater, Mars. *Geomorphology*, *240*, 83–101.

Jerolmack, D. J., Mohrig, D., Zuber, M. T., & Byrne, S. (2004). A minimum time for the formation of Holden Northeast fan, Mars. *Geophysical Research Letters*, *31*(21).

Kamada, A., Kuroda, T., Kasaba, Y., Terada, N., Nakagawa, H., & Toriumi, K. (2020). A coupled atmosphere–hydrosphere global climate model of early Mars: A 'cool and wet'scenario for the formation of water channels. *Icarus*, *338*, 113567.

Kite, E. S. (2019). Geologic constraints on early mars climate. *Space Science Reviews*, *215*(1), 10.

Kite, E. S., Lucas, A., & Fassett, C. I. (2013). Pacing early Mars river activity: Embedded craters in the Aeolis Dorsa region imply river activity spanned (1–20) Myr. *Icarus*, *225*(1), 850–855.

Kleinhans, M. G., van de Kasteele, H. E., & Hauber, E. (2010). Palaeoflow reconstruction from fan delta morphology on Mars. *Earth and Planetary Science Letters*, *294*(3-4), 378–392.

Lapôtre, M. G., & Ielpi, A. (2020). The pace of fluvial meanders on Mars and implications for the western delta deposits of Jezero crater. *AGU Advances*, *1*(2), e2019AV000141.

Lewis, K. W., & Aharonson, O. (2006). Stratigraphic analysis of the distributary fan in Eberswalde crater using stereo imagery. *Journal of Geophysical Research: Planets*, *111*(E6).

Luo, W., Cang, X., & Howard, A. D. (2017). New Martian valley network volume estimate consistent with ancient ocean and warm and wet climate. *Nature Communications*, *8*, 15766.

Malin, M. C., & Edgett, K. S. (2000). Sedimentary rocks of early Mars. *Science*, *290*(5498), 1927–1937.

Mangold, N., Ansan, V., Masson, P., & Vincendon, C. (2009). Estimate of aeolian dust

thickness in Arabia Terra, Mars: Implications of a thick mantle (> 20 m) for hydrogen detection. *Géomorphologie: relief, processus, environnement*, *15*(1), 23–32.

Matsubara, Y., Howard, A. D., & Drummond, S. A. (2011). Hydrology of early Mars: Lake basins. *Journal of Geophysical Research: Planets*, *116*(E4).

Mischna, M. A., Richardson, M. I., Wilson, R. J., & McCleese, D. J. (2003). On the orbital forcing of Martian water and CO2 cycles: A general circulation model study with simplified volatile schemes. *Journal of Geophysical Research: Planets*, *108*(E6).

Moore, J. M., Howard, A. D., Dietrich, W. E., & Schenk, P. M. (2003). Martian layered fluvial deposits: Implications for Noachian climate scenarios. *Geophysical Research Letters*, *30*(24).

Palucis, M. C., Dietrich, W. E., Williams, R. M., Hayes, A. G., Parker, T., Sumner, D. Y., ... Newsom, H. (2016). Sequence and relative timing of large lakes in Gale crater (Mars) after the formation of Mount Sharp. *Journal of Geophysical Research: Planets*, *121*(3), 472–496.

Palumbo, A. M., & Head, J. W. (2018). Early Mars Climate History: Characterizing a "Warm and Wet" Martian Climate With a 3-D Global Climate Model and Testing Geological Predictions. *Geophysical Research Letters*, *45*(19), 10–249.

Palumbo, A. M., Head, J. W., & Wordsworth, R. D. (2018). Late Noachian Icy Highlands climate model: Exploring the possibility of transient melting and fluvial/lacustrine activity through peak annual and seasonal temperatures. *Icarus*, *300*, 261–286.

Ramirez, R. M., Craddock, R. A., & Usui, T. (2020). Climate simulations of early Mars with estimated precipitation, runoff, and erosion rates. *Journal of Geophysical Research: Planets*, *125*(3), e2019JE006160.

Rosenberg, E. N., & Head, J. W. (2015). Late Noachian fluvial erosion on Mars: Cumulative water volumes required to carve the valley networks and grain size of bed-sediment. *Planetary and Space Science*, *117*, 429–435.

Salese, F., Kleinhans, M. G., Mangold, N., Ansan, V., McMahon, W., de Haas, T., & Dromart, G. (2020). Estimated Minimum Life Span of the Jezero Fluvial Delta (Mars). *Astrobiology*, *20*(8), 977–993.

Scanlon, K., Head, J., & Wordsworth, R. D. (2016). Snowmelt rates in modeled early Mars climate scenarios. In *Lunar and planetary science conference* (p. 1532).

Scanlon, K. E., Head, J. W., Madeleine, J.-B., Wordsworth, R. D., & Forget, F. (2013). Orographic precipitation in valley network headwaters: Constraints on the ancient

Martian atmosphere. *Geophysical Research Letters*, *40*(16), 4182–4187.

Schon, S. C., Head, J. W., & Fassett, C. I. (2012). An overfilled lacustrine system and progradational delta in Jezero crater, Mars: Implications for Noachian climate. *Planetary and Space Science*, *67*(1), 28–45.

Smith, D. E., Zuber, M. T., Frey, H. V., Garvin, J. B., Head, J. W., Muhleman, D. O., ... others (2001). Mars Orbiter Laser Altimeter: Experiment summary after the first year of global mapping of Mars. *Journal of Geophysical Research: Planets*, *106*(E10), 23689–23722.

Soto, A., Richardson, M., & Newman, C. (2010). Global constraints on rainfall on ancient Mars: Oceans, lakes, and valley networks. In *Lunar and Planetary Science Conference, Abstract no. 1533* (p. 2397).

Steakley, K., Murphy, J., Kahre, M., Haberle, R., & Kling, A. (2019). Testing the impact heating hypothesis for early Mars with a 3-D global climate model. *Icarus*, *330*, 169–188.

Stucky de Quay, G., Goudge, T. A., & Fassett, C. I. (2020). Precipitation and aridity constraints from paleolakes on early Mars. *Geology*, *48*(12), 1189–1193.

Toon, O. B., Pollack, J. B., Ward, W., Burns, J. A., & Bilski, K. (1980). The astronomical theory of climatic change on Mars. *Icarus*, *44*(3), 552–607.

Turbet, M., Gillmann, C., Forget, F., Baudin, B., Palumbo, A., Head, J., & Karatekin, O. (2020). The environmental effects of very large bolide impacts on early Mars explored with a hierarchy of numerical models. *Icarus*, *335*, 113419.

Urata, R. A., & Toon, O. B. (2013). Simulations of the martian hydrologic cycle with a general circulation model: Implications for the ancient martian climate. *Icarus*, *226*(1), 229–250.

von Paris, P., Petau, A., Grenfell, J., Hauber, E., Breuer, D., Jaumann, R., ... Tirsch, D. (2015). Estimating precipitation on early Mars using a radiative-convective model of the atmosphere and comparison with inferred runoff from geomorphology. *Planetary and Space Science*, *105*, 133–147.

Williams, R. M., & Weitz, C. M. (2014). Reconstructing the aqueous history within the southwestern Melas basin, Mars: Clues from stratigraphic and morphometric analyses of fans. *Icarus*, *242*, 19–37.

Wordsworth, R. D. (2016). The climate of early Mars. *Annual Review of Earth and Planetary Sciences*, *44*, 381–408.

Wordsworth, R. D., Forget, F., Millour, E., Head, J., Madeleine, J.-B., & Charnay, B. (2013). Global modelling of the early martian climate under a denser CO2 atmosphere: Water cycle and ice evolution. *Icarus*, *222*(1), 1–19.

Wordsworth, R. D., Kerber, L., Pierrehumbert, R. T., Forget, F., & Head, J. W. (2015). Comparison of "warm and wet" and "cold and icy" scenarios for early Mars in a 3-D climate model. *Journal of Geophysical Research: Planets*, *120*(6), 1201–1219.

Wordsworth, R. D., Knoll, A. H., Hurowitz, J., Baum, M., Ehlmann, B. L., Head, J. W., & Steakley, K. (2021). A coupled model of episodic warming, oxidation and geochemical transitions on early Mars. *Nature Geoscience*, *14*(3), 127–132.